Monthly Notices
of the
ROYAL ASTRONOMICAL SOCIETY

MNRAS **469,** S29–S38 (2017)
Advance Access publication 2017 April 10

doi:10.1093/mnras/stx868

Lower hybrid waves at comet 67P/Churyumov–Gerasimenko

M. André,[1⋆] E. Odelstad,[1,2⋆] D. B. Graham,[1] A. I. Eriksson,[1⋆] T. Karlsson,[3] G. Stenberg Wieser,[4] E. Vigren,[1] C. Norgren,[1,2] F. L. Johansson,[1,2] P. Henri,[5] M. Rubin[6] and I. Richter[7]

[1]*Swedish Institute of Space Physics, Uppsala, Sweden*
[2]*Department of Physics and Astronomy, Uppsala University, Uppsala, Sweden*
[3]*Department of Space and Plasma Physics, School of Electrical Engineering, KTH Royal Institute of Technology, Stockholm, Sweden*
[4]*Swedish Institute of Space Physics, Kiruna, Sweden*
[5]*Laboratoire de Physique et Chimie de l'Environnement et de l'Espace, Orleans, France*
[6]*Physikalisches Institut, University of Bern, Bern, Switzerland*
[7]*TU – Braunschweig, Institute for Geophysics and Extraterrestrial Physics, Braunschweig, Germany*

Accepted 2017 April 5. Received 2017 March 31; in original form 2017 March 31

ABSTRACT

We investigate the generation of waves in the lower hybrid frequency range by density gradients in the near plasma environment of comet 67P/Churyumov–Gerasimenko. When the plasma is dominated by water ions from the comet, a situation with magnetized electrons and unmagnetized ions is favourable for the generation of lower hybrid waves. These waves can transfer energy between ions and electrons and reshape the plasma environment of the comet. We consider cometocentric distances out to a few hundred km. We find that when the electron motion is not significantly interrupted by collisions with neutrals, large average gradients within tens of km of the comet, as well as often observed local large density gradients at larger distances, are often likely to be favourable for the generation of lower hybrid waves. Overall, we find that waves in the lower hybrid frequency range are likely to be common in the near plasma environment.

Key words: plasmas – waves – comets: general.

1 INTRODUCTION

Many plasma phenomena may occur in the surroundings of comets. Comets consist to a large extent of volatile material such as ice from H_2O, CO and CO_2. The ice can sublimate when the comet is close enough to the sun and produce outflowing gas. Photoionization of this gas by solar extreme ultraviolet (EUV) radiation and also ionization by electron impact and charge exchange reactions contribute to a comet plasma surrounding somewhat similar to a planetary ionosphere (Biermann 1951; Alfvén 1957; Cravens et al. 1987; Altwegg, Balsiger & Geiss 1999; Glassmeier et al. 2007; Edberg et al. 2015; Hässig et al. 2015; Nilsson et al. 2015a,b; Odelstad et al. 2015; Galand et al. 2016; Yang et al. 2016; Eriksson et al. 2017).

The environment of a comet includes several sources of free energy for plasma phenomena such as waves and currents that can redistribute energy between particle populations and reshape the environment. We concentrate on waves in the lower hybrid frequency range since these waves can transfer energy between ions and electrons (Krall & Liewer 1971; Huba, Gladd & Papadopoulos 1977; Bale, Mozer & Phan 2002; Vaivads et al. 2004; Zhou et al. 2009; Khotyaintsev et al. 2011; Norgren et al. 2012; Graham et al. 2017). Such waves have recently been observed near comet 67P/Churyumov–Gerasimenko (67P) (Karlsson et al. 2017; Stenberg Wieser 2017) by the dual Langmuir probe instrument LAP on the *Rosetta* spacecraft (Carr et al. 2007; Eriksson et al. 2007; Taylor et al. 2015). For a significant part of the *Rosetta* mission, the spacecraft is located at distances from the comet where the electrons are magnetized while the ions are essentially unmagnetized (typically distances of tens to hundreds of kilometres). This is a favourable situation for the generation of lower hybrid waves.

Plasma phenomena near a comet may include interaction between various plasma populations originating from the comet, or between particles from the solar wind and from the comet. Sources of free energy include the relative motion between comet and solar wind particles, and gradients in both velocity and real space. One example is that neutral particles from a comet being ionized in the solar wind are picked up by the solar wind motion. This can result in gradients in ion velocity space (non-Maxwellian and non-gyrotropic distributions) resulting in waves acting back on the distribution function, as observed near comet 1P/Haley (Oya et al. 1986; Richardson et al. 1989; Neugebauer 1990). (For 67P this would typically correspond to length-scales of at least the ion gyroradius, at least several

⋆ E-mail: mats.andre@irfu.se (MA); elias.odelstad@irfu.se (EO); aie@irfu.se (AIE)

hundred kilometres.) These pick-up ions can form unstable distributions without directly interacting with solar wind ions (Coroniti et al. 1986; Galeev et al. 1988), while in other cases interaction with solar wind ions is essential (Galeev et al. 1988; Shapiro et al. 1999). A similar situation may occur in the case of Venus and Mars, without global magnetic fields, when solar wind protons interact with heavy ions such as O^+ of planetary origin (Shapiro et al. 1995; Sauer et al. 1998; Bingham et al. 2010).

A situation somewhat similar to a comet surrounding was artificially created by the AMPTE (Active Magnetospheric Particle Tracer Explorers) mission. Here barium or lithium was explosively released and ionized by solar EUV radiation. These new ions may interact with the solar wind (Bingham et al. 1991). In the region dominated by newly released ions, gradients due to an outward decrease of plasma density may be important for wave generation. On short time and spatial scales (compared to the heavy ion gyroperiod and gyroradius), the ions are essentially unmagnetized and expand radially outwards, while the electrons are frozen-in. The density gradient can cause a diamagnetic drift of ions and electrons. In addition, ambipolar electric fields affect the particle motion (Madanian et al. 2016). In this situation of unmagnetized ions, frozen-in electrons and density gradients in an expanding plasma cloud, waves around the lower hybrid frequency are expected, similar to the near plasma environment of a comet (Winske 1988, 1989). Another more extreme artificial release of energy, the 1962 Starfish nuclear burst in the ionosphere, can also be compared to some properties of comets (Dyal 2006).

A region of frozen-in electrons and unmagnetized ions is also encountered in the ion diffusion region of magnetic reconnection (Priest & Forbes 2000; Fujimoto, Shinohara & Kojima 2011). This region has been explored using theory and simulations (Hesse et al. 2016) and detailed observations by multispacecraft missions in near-Earth space such as Cluster and MMS (Paschmann, Øieroset & Phan 2013; Burch et al. 2016). These observations allow detailed comparison with numerical calculations showing that realistic wave generation mechanisms include both interaction between ion populations of different temperature drifting relative to each other, and also density gradients causing a current due to diamagnetic drift (Graham et al. 2017). While dedicated high-resolution multispacecraft missions can give a detailed picture of an ion diffusion region, these encounters typically last a few seconds. *Rosetta* has spent 2 yr investigating the surrounding of comet 67P. We use models based on these observations, and detailed observations during one event, to investigate how common lower hybrid waves can be in the near plasma environment.

There are some observations of waves in the lower hybrid frequency range reported from spacecraft fly-bys of the comets 1P/Halley (Klimov et al. 1986; Galeev et al. 1988) and 21P/Giacobini–Zinner (Scarf et al. 1986; Scarf 1989). These waves are often observed in the magnetosheath region and are likely to be generated by pick-up ions. The *Rosetta* 2-yr investigation of 67P provides a good opportunity to study the waves in the near plasma environment of a comet. Observations include magnetic field observations of large-amplitude compressional waves around 40 mHz (Koenders et al. 2016; Richter et al. 2015, 2016), mirror modes (Volwerk et al. 2016) and ion acoustic waves (Gunell et al. 2017). The first electric-field observations around 67P include waves around the lower hybrid frequency (typically a few Hz). These are associated with sharp local density gradients (Karlsson et al. 2017; Stenberg Wieser 2017). We use *Rosetta* observations to investigate the near plasma environment of 67P, out to cometocentric distances of hundreds of km, including plasma density gradients. We find that when the electron motion is not significantly interrupted by collisions with neutrals, large local density gradients, as well average large gradients close to the comet, are often favourable for the generation of lower hybrid waves.

2 GENERAL PLASMA MODEL

To estimate when the conditions in the near plasma environment of a comet are favourable for the generation of lower hybrid waves, a reasonably simple geometry is used. The real comet nucleus ejects gas and jets of dust in different directions, causing an inhomogeneous time-varying three-dimensional environment (Hässig et al. 2015). Also the plasma environment is time-varying and three-dimensional (Edberg et al. 2015; Odelstad et al. 2015; Eriksson et al. 2017), Fig. 1(a). This plasma interacts with magnetic field originating from the solar wind, while sometimes a magnetic cavity is formed around the comet (Goetz et al. 2016; Mandt et al. 2016).

To investigate some phenomena, a simplified two-dimensional situation may be used, Fig. 1(b). Here, the comet is represented by a long cylinder in the same direction as the magnetic field and the outflow is assumed to be steady and the same in all directions. This is reasonable when we are interested in average conditions and phenomena occurring mainly perpendicular to the magnetic field. We investigate when the density gradients around a comet are large enough to cause instabilities of lower hybrid waves with wave vectors (and electric fields) nearly perpendicular to the magnetic field, so this is a useful approximation.

To further simplify, we consider a one-dimensional model with a magnetic field and densities varying as a function of distance from the comet nucleus, Fig. 1(c). This local approximation is useful when the waves we consider have a wave vector nearly perpendicular to both the magnetic field and the density gradients, and a wavelength much shorter than the distance to the comet. This is the case for the lower hybrid waves we investigate.

3 THE NEAR PLASMA ENVIRONMENT OF COMET 67P

We consider situations when the near plasma environment of 67P out to distances from the comet of at least a few hundred kilometres is dominated by plasma from the comet and by a magnetic field of solar wind origin. At *Rosetta*'s position, cometary ions dominated the local environment for most of the mission (Nilsson et al. 2015b; Odelstad et al. 2015; Yang et al. 2016; Stenberg Wieser 2017), with no solar wind protons observed closer to the Sun than about 1.7 au (Behar et al. 2017). A magnetic field of tens of nT is typically observed near the comet, while sometimes a magnetic cavity is found (Goetz et al. 2016; Goetz et al. 2017). This magnetic field originates in the solar wind since the comet nucleus is not magnetized (Auster et al. 2015). It is clear that (large-scale) mass-loading of the solar wind by pick-up ions from the comet will slow down the solar wind and cause a so-called pile-up (local increase) of the magnetic field near the comet, e.g. Neubauer (1987). However, the situation in the near plasma environment may be complicated. When there is very little outgassing from the comet, frozen-in plasma not hitting the comet nucleus can pass essentially unaffected. When the near plasma environment is dominated by cometary plasma, current systems are set up to adjust to the solar wind magnetic field strength and motion, and two- and three-dimensional models should be considered. In some situations, electrons frozen-in to a magnetic field moving relative to cometary ions may be important for wave instabilities. Rather, in the following we investigate the case when

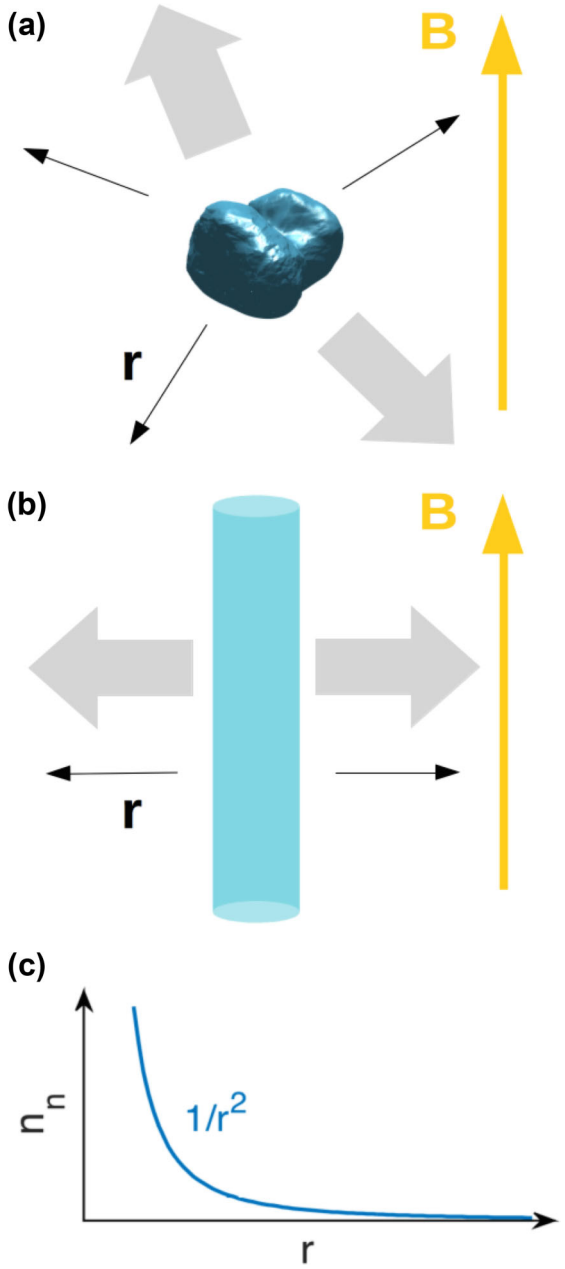

Figure 1. Models of the comet environment. (a) Sketch of the three-dimensional comet environment; (b) sketch of a two-dimensional model of the environment, useful for phenomena occurring mainly perpendicular to the magnetic field; (c) sketch of the model we use, useful for waves with wave vectors and electric field mainly perpendicular to the magnetic field, and with wavelengths short compared to distance from the point of interest to the comet. The density of neutral gas n_n is indicated.

the magnetic field motion relative to the comet nucleus can be ignored.

To model the inner coma plasma, we use the simplified model by Eriksson et al. (2017). Neutral gas flows outward from the comet with a velocity of about 0.7 km s^{-1} (Gulkis et al. 2015), with the density decreasing as r^{-2}

$$n_n(r) \approx n_0 \left(\frac{R}{r}\right)^2, \tag{1}$$

where n_0 is the neutral gas density at the surface of a comet with radius R, and n_n is the density at the cometocentric distance r. Assuming that steady ionization by solar EUV radiation dominates, this gives a peak in plasma density at some cometocentric distance, and a decrease of this density as r^{-1} at large distances (since the density of neutrals is typically much higher than the plasma density):

$$n_e(r) \approx n_0 \frac{\nu R}{u}\frac{R}{r}\left(1-\frac{R}{r}\right), \tag{2}$$

where n_e is the electron density at some distance r, ν is an ionization frequency depending on the distance to the sun and u is the outflow velocity of the plasma (Haser 1957; Mandt et al. 2016; Eriksson et al. 2017; Vigren & Eriksson 2017; Vigren 2017). Assuming that the plasma is dominated by water ions from the comet, ion–electron pairs are created with particle energies of less than 0.1 and about 12 eV, respectively (due to conservation of momentum). When the density is high enough close to the nucleus, neutral-electron collisions will cool the electrons to temperatures of 0.1 eV or less. Beyond some distance r_{ce} the electrons are not efficiently cooled, and a mixture of cool (0.1 eV) and warm (5–10 eV) electrons are observed (Edberg et al. 2015; Mandt et al. 2016; Eriksson et al. 2017). Collisions between neutrals and ions are important out to larger distances. We investigate the region where electron-neutral collisions can be neglected, and warm electrons are present and magnetized, while the ions are unmagnetized due to collisions and their large gyroradius. This is a region favourable for lower hybrid waves and is where *Rosetta* spend much of its time during the 2 yr investigation of 67P (Mandt et al. 2016). We use three populations to model the plasma, cold and warm electrons, and H_2O^+ ions

$$n_{ew}(r) \approx n_0 \frac{\nu R}{u}\frac{R}{r}\left(1-\frac{r_{ce}}{r}\right) \qquad r \geq r_{ce}, \tag{3}$$

$$n_{ec}(r) \approx n_e(r_{ce})\frac{r_{ce}^2}{r^2} = n_0 \frac{\nu R}{u}\frac{R r_{ce}}{r^2} \qquad r \geq r_{ce}, \tag{4}$$

$$n_i(r) \approx n_0 \frac{\nu R}{u}\frac{R}{r}\left(1-\frac{R}{r}\right), \tag{5}$$

where n_{ew}, n_{ec} and n_i are the densities of warm and cold electrons, and ions, respectively (Eriksson et al. 2017). For distances smaller than r_{ce}, the electron motion is disrupted by collisions and lower hybrid waves are likely to be heavily damped.

To estimate the cometocentric distance r_{ce} beyond which neutral-electron collisions can be neglected, we set this limit where the neutral density n_n has decreased so that r_{ce} equals the collision length

$$r_{ce} = \sigma_{ne} n_0 R^2 = \sigma_{ne} n_n r^2, \tag{6}$$

where $\sigma_{ne} = 5 \times 10^{-16}$ cm^{-2} is the electron-neutral momentum transfer cross-section (for 5 eV electrons) (Itikawa & Mason 2005; Mandt et al. 2016). For *Rosetta* at 67P, this gives distances varying from the surface of the nucleus at 3 au out to around 100 km around perihelion. We use this simple model but note that the electromagnetic field environment will also affect the energetics of the electrons. An ambipolar electric field, caused by the low mass electrons moving away from the heavier ions, will decelerate electrons and may even attract such particles back to denser regions with enhanced collision probabilities. In the direction perpendicular to the magnetic field, outflowing unmagnetized ions move relative to the magnetized electrons, further complicating the particle motion. Here the frozen-in electrons adjust to keep charge neutrality

as the ions flow outward, which probably involves two- or three-dimensional current systems. The model of the average electron density and temperature we use is simplified, but we consider the model useful since the predicted mixture of cold and warm electrons is consistent with *Rosetta* observations at 67P (Edberg et al. 2015; Eriksson et al. 2017).

Collisions between ions and neutrals are important out to larger cometocentric distances, with lower density, due to a collision cross-section different from that of the electrons (Mandt et al. 2016; Eriksson et al. 2017). This interaction is mainly due to charge-exchange and prevents acceleration to high energies. In the simplest approximation, the ions should stay cold (less than 0.1 eV) and flow together with the neutrals. However, recent estimates show that realistic ambipolar electric fields and collision rates (electrons moving outward in a one-dimensional model without magnetic field) can accelerate ions to energies of a few eV, mainly in the outward direction (Vigren & Eriksson 2017). We note that in the direction nearly perpendicular to the magnetic field we consider the situation is more complicated since the unmagnetized ions can move more freely than the magnetized electrons. In addition waves, including lower hybrid waves, can also energize the ions. Hence, ion energization up to at least a few eV seems plausible in the region of frequent ion-neutral collisions we consider (also without an electric field induced by the solar wind). Observations in the near plasma environment of 67P dominated by water group ions are typically consistent with average energies of at least 5–10 eV (Nilsson et al. 2015a,b; Stenberg Wieser 2017). Considering recent theoretical and observational investigations, we use ion temperatures of 5–10 eV as a realistic input to models of the average plasma environment.

Since the ions are not very strongly coupled to the neutral gas via collisions, the outflow velocities of ions and neutrals may differ. Energization of the ions by an outward ambipolar electric field can also affect the outward bulk velocity, corresponding to energies of a few eV (Vigren & Eriksson 2017). Recent estimates combining observations from the LAP, mutual impedance probe (MIP) and COPS instruments (Balsiger et al. 2007; Eriksson et al. 2007; Trotignon et al. 2007) give outflow velocities of a few km s^{-1} (Vigren 2017) (at a heliospheric distance of 1.24 au and cometocentric distances of 200–250 km). In the following, we do not use the typical outflow velocity of the neutral [about 1 km s^{-1}, Gulkis et al. (2015)], but rather use $u = 3$ km s^{-1} as the ion outflow velocity.

The magnetic field induced by the diamagnetic drift of electrons and ions around the comet will affect the whole near plasma environment of the comet. The magnitude of the induced field can be similar in magnitude to the magnetic field of solar wind origin, and the induced field may be essential for the formation of a magnetic cavity around the comet. Rather, we investigate when density variations are essential for the generation of lower hybrid waves, and in our local model assume a constant magnetic field. Our goal is to find when the order of magnitude of the density gradients is high enough for the generation of lower hybrid waves.

4 THEORY OF LOWER HYBRID WAVES

The lower hybrid frequency ω_{LH} is

$$\omega_{LH} = \sqrt{\frac{\Omega_{ce}\Omega_{ci}}{1+\frac{\Omega_{ce}}{\omega_{pe}}}} \approx \sqrt{\Omega_{ce}\Omega_{ci}}, \tag{7}$$

where ω_{pe} is the electron plasma frequency, and Ω_{ce} and Ω_{ci} are the gyrofrequencies of electrons and ions, respectively. The approximate relation is valid for the relatively dense plasmas we consider. For H_2O^+ ions and for typical magnetic fields in our study of 10–50 nT, waves observed at the lower hybrid frequency would appear at $f_{LH} = \omega_{LH}/2\pi$ of about 2–10 Hz.

We calculate the frequency, growth rate and wavelength for waves around the lower hybrid frequency in a plasma with density gradients (the lower hybrid drift instability, LHDI). We assume that the waves propagate perpendicular to both the magnetic field B and the density gradient, and solve the relevant local dispersion equation (Krall & Liewer 1971; Davidson & Gladd 1975; Graham et al. 2017):

$$0 = 1 - \frac{\omega_{pi}^2}{k^2 v_i^2} Z'\left(\frac{\omega}{k v_i}\right) + \frac{\omega_{pew}^2}{\Omega_{ce}^2}\frac{1 - I_0(b)\exp(-b)}{b} + \frac{2\omega_{pew}^2}{k^2 v_{ew}^2}\frac{I_0(b)\exp(-b) k V_{de}}{\omega - k V_E} + \frac{\omega_{pec}^2}{\Omega_{ce}^2}, \tag{8}$$

where $V_{de} = -v_{ew}^2/(2\Omega_{ce}) n_{ew}^{-1} \partial n_{ew}/\partial r$ is the diamagnetic drift of warm electrons, $\omega_{pi,\,pew,\,pec}$ are the ion, warm electron and cold electron plasma frequencies, $v_{i,\,ew}$ are the ion and warm electron thermal speeds, V_E is the $\boldsymbol{E} \times \boldsymbol{B}$ drift, $b = k^2 v_{ew}^2/(2\Omega_{ce}^2)$, Z' is the derivative of the plasma dispersion function, I_0 is the modified Bessel function of first kind of order zero. Equation (8) corresponds to the ion rest frame, so we assume $V_E = -V_{di}$, where V_{di} is the ion diamagnetic drift, corresponding to force balance in the absence of local acceleration. We assume that there is no diamagnetic drift associated with the cold electron population and that the diamagnetic drifts develop due to density changes, while B, T_{ew} and T_i are assumed to be constant.

To model the lower hybrid wave properties as a function of position from the comet, we solve equation (8) analytically by assuming small drifts $V_E < v_i$. By expanding Z' in the limit $v_{ph} = \omega/k \ll v_i$, where v_{ph} is the phase speed, we obtain (Davidson & Gladd 1975)

$$\omega_r = k V_E \left(1 - \frac{2\omega_{pew}^2 I_0(b)\exp(-b) V_{de}}{k^2 v_{ew}^2 V_E} \times \left[1 + \frac{\omega_{pi}^2}{k^2 v_i^2} + \frac{\omega_{pew}^2}{\Omega_{ce}^2}\frac{1 - I_0(b)\exp(-b)}{b} + \frac{\omega_{pec}^2}{\Omega_{ce}^2}\right]^{-1}\right), \tag{9}$$

$$\gamma = \sqrt{\pi}\frac{T_e}{T_i}\frac{(\omega_r - k V_E)^2}{|k| v_i}\frac{\omega_r}{I_0(b)\exp(-b) k V_{de}}. \tag{10}$$

In the following, we use equations (9) and (10) when the typical cross-field drifts are below v_i, and solve equation (8) numerically when needed.

For comparison, the modified two stream instability (MTSI) is also considered. In this case, the outflowing unmagnetized ions drift perpendicular to the magnetic field, relative to the magnetized electrons (McBride et al. 1972; Wu et al. 1983). We will use a modified version of equation 17 in Wu et al. (1983).

5 MODELS OF THE NEAR PLASMA ENVIRONMENT AND LOWER HYBRID WAVES

In the following, we investigate two near plasma environments of 67P, typical for two heliocentric distances.

5.1 Model 1 (1.7 au)

The first model we consider is consistent with typical parameters for 67P at about 1.7 au when the activity is rather high

(Mandt et al. 2016; Eriksson et al. 2017; Karlsson et al. 2017). An event with waves in the lower hybrid frequency range at this heliocentric distance is also discussed in the next section.

The following parameters are used in equations (3)–(5): $R = 2$ km, $n_0 = 2 \times 10^{11}$ cm^{-3}, $u = 3$ km s^{-1}, $\nu = 2.4 \times 10^{-7}$/s, $T_i = 10$ eV, $T_{ec} = 0.1$ eV, $T_{ew} = 5$ eV, $B_0 = 30$ nT, $r_{ce} = 40$ km, where we use the notation temperature although all populations are not well described by Maxwellian distributions.

The ionization rate ν is calculated for photoionization at this heliocentric distance (Vigren et al. 2015). The ion and electron temperatures, and the magnetic field, are consistent with *Rosetta* observations at 1.7 au discussed later.

The model is illustrated in Fig. 2. Here we show the density of all plasma components, and for the warm electrons also the inverse of the gradient scalelength L normalized to the gyroradius of these electrons ρ_{ew}:

$$L = \left(\frac{1}{n} \frac{dn}{dr} \right)^{-1}, \quad (11)$$

where a large $(L/\rho_{ew})^{-1}$ indicates a steep gradient and the possibility for wave growth. (Here, $\rho_{ew} \approx 250$ m.)

We do not consider wave growth at smaller cometocentric distances than $r_{ce} = 40$ km since collisions significantly disrupting the electron motion are likely to damp lower hybrid waves. To investigate the LHDI instability, use equations (9) and (10) since the diamagnetic drifts are smaller than $v_i \approx 10$ km s^{-1} for the relevant distances. Maximum wave growth rate is obtained approximately at the most negative density gradient of the warm electrons, at about 100 km.

However, the maximum growth rate is not large, about $\gamma/\omega_{LH} = \gamma/(2\pi f_{LH}) \approx 0.01$, which for a lower hybrid frequency f_{LH} of 5 Hz gives 10 e-foldings of wave amplitude (from existing noise) in 30 s. During this time interval the conditions can change, including an outward drift of about 100 km to regions with much lower gradients and wave growth. We find that the waves are growing in this global density gradient, but waves with significant amplitudes would more likely be associated with sharper local gradients if generated by this mechanism.

We also consider the MTSI, to investigate if this gives higher growth rates for waves in the lower hybrid frequency range. We solve equation 17 in Wu et al. (1983) modified to include two electron populations, for the following parameters. These are mainly consistent with Model 1 at 130 km (cometocentric distance where local *Rosetta* observations are discussed below) $n_i = 580$ cm^{-3}, $n_{ew} = 440$ cm^{-3}, $n_{ec} = 140$ cm^{-3}, $T_i = 5$ eV, $T_{ec} = 0.1$ eV, $T_{ew} = 10$ eV, $u = 3$ km s^{-1}, $B_0 = 30$ nT, where we have modified the ion and warm electron temperatures to obtain slightly higher growth rates. The dispersion relation was solved for k-vectors close to perpendicular to the magnetic field. The maximum growth was found for $\theta = 89.87$ deg. As with the LHDI case, maximum growth corresponds to about $\gamma/(2\pi f_{LH}) \approx 0.01$ ($k\rho_{ew} \approx 2$). Again, the growth rate is rather small. This instability does not depend on local gradients and can possibly provide growth as the ions drift outward. However, the instability requires wave growth at f_{LH} during many seconds and is less likely to provide growth to high amplitudes.

5.2 Model 2 (2.3 au)

We also consider a model typical for the near plasma environment at a heliocentric distance of about 2.3 au (Edberg et al. 2015; Odelstad et al. 2015). The lower activity at this larger heliocentric distance means that the density is smaller and the electron-neutral collision rate is small enough that there may be no significant electron cooling. Thus, all electrons are warm (few eV) and there may be sharp density gradients close to the comet. The following parameters will be used: $R = 2$ km, $n_0 = 9 \times 10^9$ cm^{-3}, $u = 3$ km s^{-1}, $\nu = 1.3 \times 10^{-7}$/s, $T_i = 10$ eV, $T_{ew} = 5$ eV, $B_0 = 15$ nT, $r_{ce} = 2$ km (surface of the comet nucleus, i.e. all electrons are warm, 5 eV)

The model is illustrated in Fig. 3. To investigate the LHDI instability we use equations (9) and (10) for large distances, above about 100 km, when the diamagnetic drift is small, and

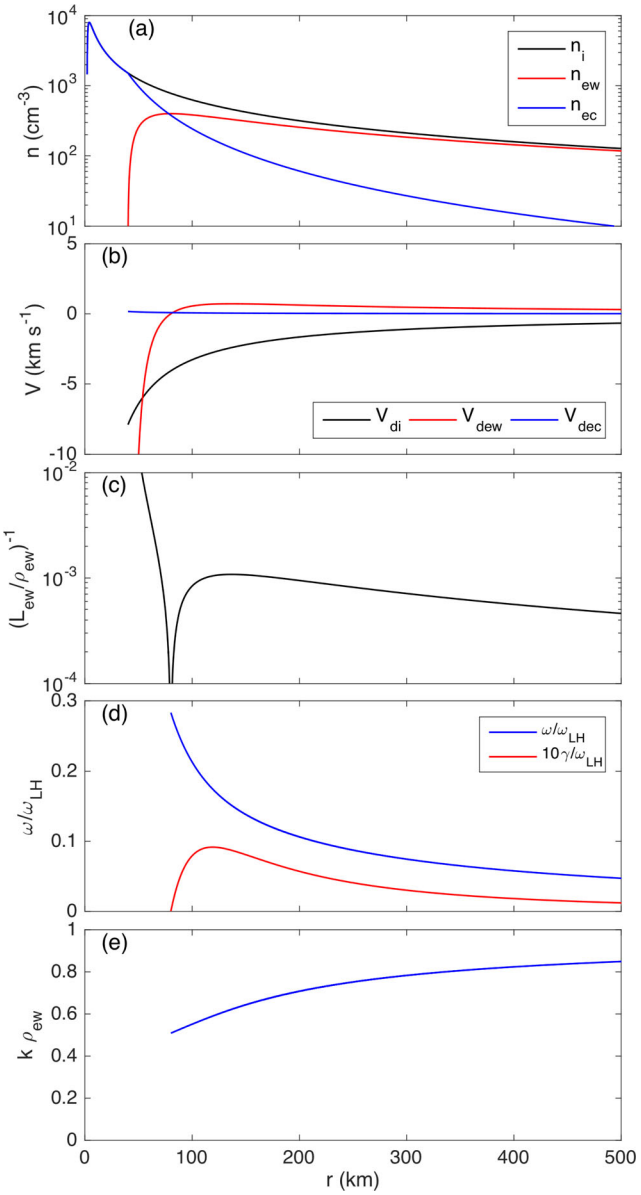

Figure 2. Model of the near plasma environment of comet 67P, at an heliocentric distance of 1.7 au. (a) The density of cold (0.1 eV), warm (5 eV) electrons and ions (10 eV) as a function of distance from the comet. Close to the comet (less than 40 km) electrons are cooled by collisions with the neutral gas. (b) Diamagnetic drift velocity. (c) Inverse of the gradient scalelength for warm electrons. (d) Real and imaginary wave frequency for maximum γ (maximum wave growth) at each distance. (e) Corresponding wave vector. Waves in the lower hybrid frequency range are growing but the growth rates are small.

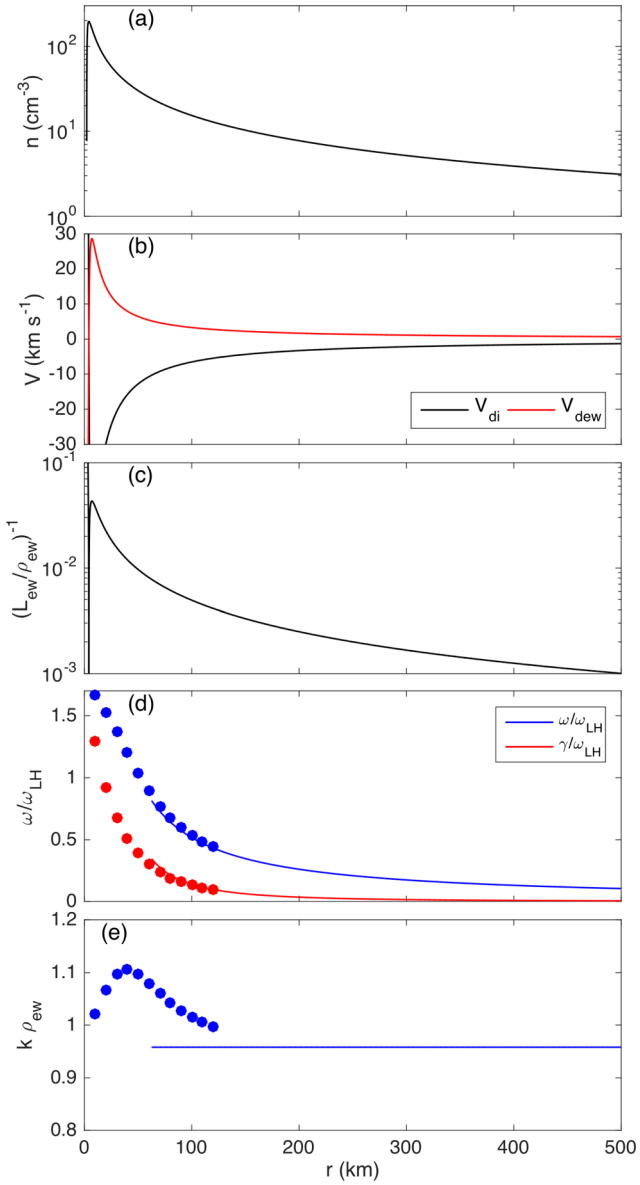

Figure 3. Model of the near plasma environment of comet 67P, at an heliocentric distance of 2.3 au. The panels are the same as for Fig. 2. Note that due to a lower collision rate, there are no cold electrons, and there is a region with large density gradients not dominated by collisions close to the comet. For large distances, equations (9) and (10) are used (solid lines), while for small distances and large drift velocities equation (8) has been solved numerically (circles). Large wave growth rates are predicted close to the comet.

numerically solve equation (8) for smaller distances. In this model sharp gradients not dominated by electron-neutral collisions are found. The corresponding wave growth rates close to the comet, within tens of km, are also large. Here $\gamma \approx \omega_{LH}$ indicating several e-foldings of wave amplitude within a second, and within a few km of ion drift. This wave growth is likely to be limited by non-linear effects not included here. We find that waves in the lower hybrid frequency range are growing due to large density gradients close to the comet.

6 OBSERVATIONS OF THE NEAR PLASMA ENVIRONMENT AND LOWER HYBRID WAVES (1.7 AU)

We investigate observations from one event when waves near the lower hybrid frequency were observed by the instruments in the *Rosetta* Plasma Consortium RPC (Carr et al. 2007; Eriksson et al. 2007; Nilsson et al. 2007; Trotignon et al. 2007), Fig. 4. This interval was selected since the LAP dual Langmuir probe instrument was in a mode suitable for electric-field observations, waves in the lower hybrid frequency range were observed, ICA ion observations were available at high time resolution (4 s) (Stenberg Wieser 2017) and data from additional RPC instruments were also available (Karlsson et al. 2017). The observations were obtained at a heliocentric distance of about 1.7 au, and a cometocentric distance of about 130 km, see also Model 1.

Fig. 4(a) shows the signals of the two individual probes of the LAP instrument on *Rosetta*, the small differences of which are associated with the measured electric field (Eriksson et al. 2007; Karlsson et al. 2017). The individual probe signals themselves are good approximations of the negative of the spacecraft potential with respect to the surrounding plasma (Odelstad 2017). Fig. 4(b) shows a spectrogram of the electric-field signal. The red line indicates the H_2O^+ lower hybrid frequency calculated from the magnetic field. Fig. 4(c) shows the fluctuating electric field (the low-frequency component is removed by subtracting a running mean, using a 0.5 s window). Fig. 4(d) shows the magnetic field, Fig. 4(e) shows an energy–time spectrogram of water group ions. Here a high time resolution mode is used, providing one energy sweep (5–95 eV) every 4 s. The data shown have been corrected for a 9.7 eV offset in the energy table (Stenberg Wieser 2017). The remaining low-energy cut-off is mainly due to acceleration of ions into the detector caused by the negative spacecraft potential. Compensating for the effect of the spacecraft potential and calculating the average energy during the event in Fig. 4 gives about 5–10 eV. Some small fraction of the ions reaching energies of at least 100 eV have probably left the near environment of the comet, been accelerated, and then returned.

Fig. 4(f) shows plasma density from the mutual impedance probe (MIP) instrument with a time resolution of about 4 s, sometimes with short data gaps (Trotignon et al. 2007), and the probe potentials from LAP, similar to panel a, obtained at 60 Hz (Eriksson et al. 2007). The spacecraft potential depends on the electron temperature and density (Fahleson 1967; Pedersen et al. 2008; Lybekk et al. 2012; Odelstad et al. 2015). The LAP and MIP data sets have been compared, indicating an average electron temperature during this event of 5 eV. Using this temperature, the relation between density and probe potential in Fig. 4(f) was obtained. When the agreement between LAP and MIP density estimates is not good, including around 16:40 UTC, this may be due to, e.g. a different electron temperature during this time. The main reason for including LAP probe data as an indicator of density is to obtain high resolution and low noise for estimates of density gradients. For comparison we note that the neutral gas density obtained by the COPS instrument (Balsiger et al. 2007; Mandt et al. 2016) is slowly varying during this time interval, at 4.2–4.6 $\times$ 10^7 cm^{-3}, with none of the sharp variations seen in the plasma data from LAP and MIP. Fig. 4(g) shows plasma density gradients estimated from LAP spacecraft potential data, using averages over 1 s. Averaging is used to remove rapid fluctuations that may be due to the waves themselves, since we are interested in density gradients potentially causing the waves.

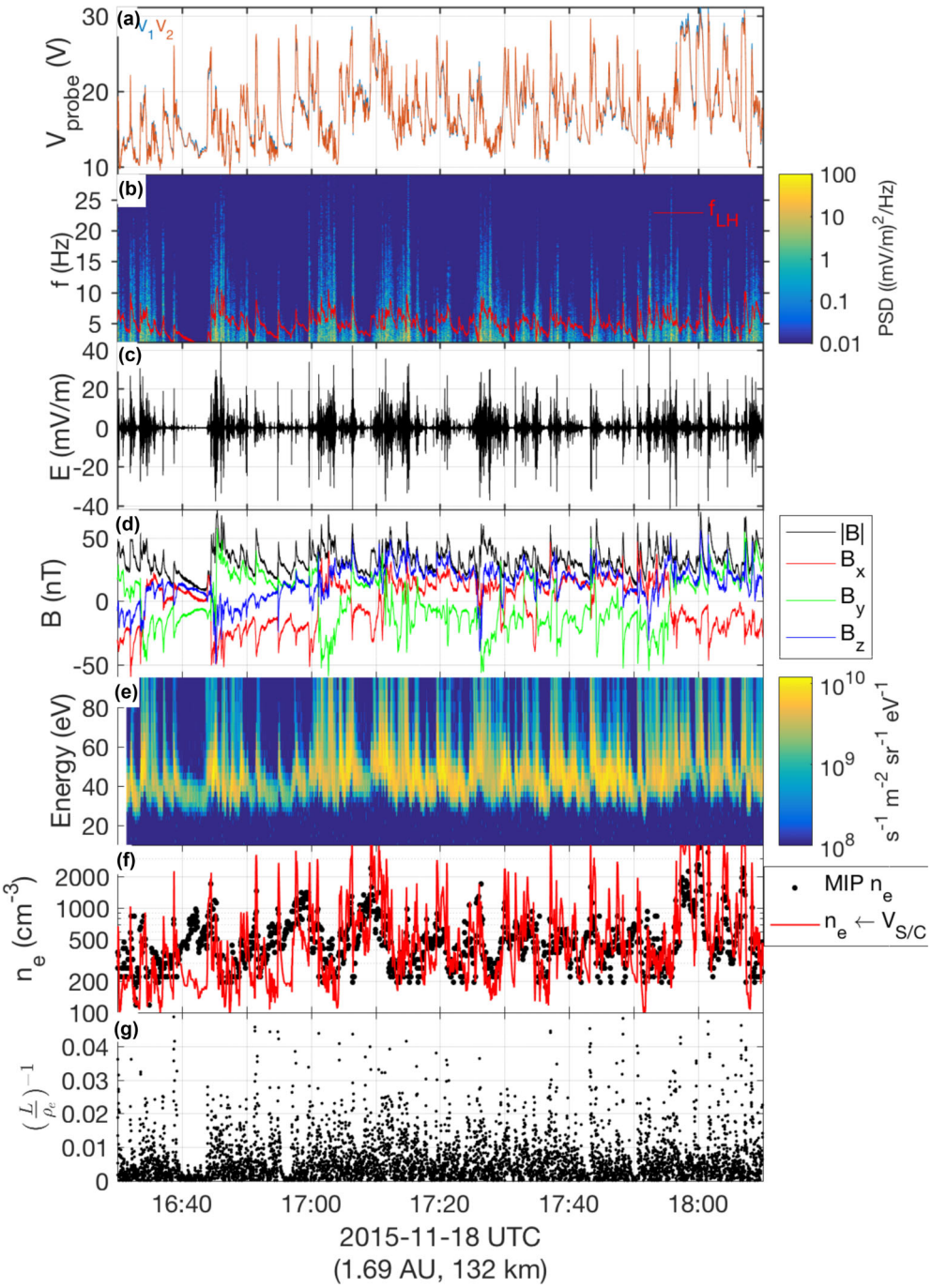

Figure 4. Observations by *Rosetta* at a heliocentric distance of about 1.7 au and a cometocentric distances of about 130 km, including waves in the lower hybrid frequency range and density gradients. The panels show (a) individual probe signals (the LAP instrument); (b) spectrogram of the electric-field signal, with the calculated lower hybrid frequency of water ions indicated (LAP and MAG); (c) electric field, with the low-frequency component removed (LAP); (d) three components of the magnetic field, and the total field (MAG); (e) spectrogram of water group ions (ICA); the low energy cut-off is mainly due to the spacecraft potential; (f) plasma density (MIP), together with high-resolution probe potentials, similar to panel (a) (LAP) indicating sharp gradients; (g) plasma density gradients (LAP).

Assuming a constant electron temperature, the plasma density gradient can be written

$$\left(\frac{1}{n_\mathrm{e}}\frac{\mathrm{d}n_\mathrm{e}}{\mathrm{d}x}\right)^{-1} = \left(\frac{e}{k_\mathrm{B}T_\mathrm{e}}\frac{\mathrm{d}V_\mathrm{SC}}{\mathrm{d}x}\right)^{-1}, \tag{12}$$

where e is the electron charge, k_B is Boltzmanns constant, V_SC is the spacecraft potential, and in this equation T_e is in K. To obtain Fig. 4(g), we use $T_\mathrm{e} = 5$ eV, and $\mathrm{d}x = u\mathrm{d}t$, with $u = 3\,\mathrm{km\,s^{-1}}$, as discussed above.

Large density gradients are observed, compared to the typical average gradients at cometocentric distances larger than tens of km in our models. Several wave packets with amplitudes of more than 40 mV m^{-1} peak-to-peak are observed, Fig. 4(c), often occurring at large density gradients. Two wave packets are shown in higher time

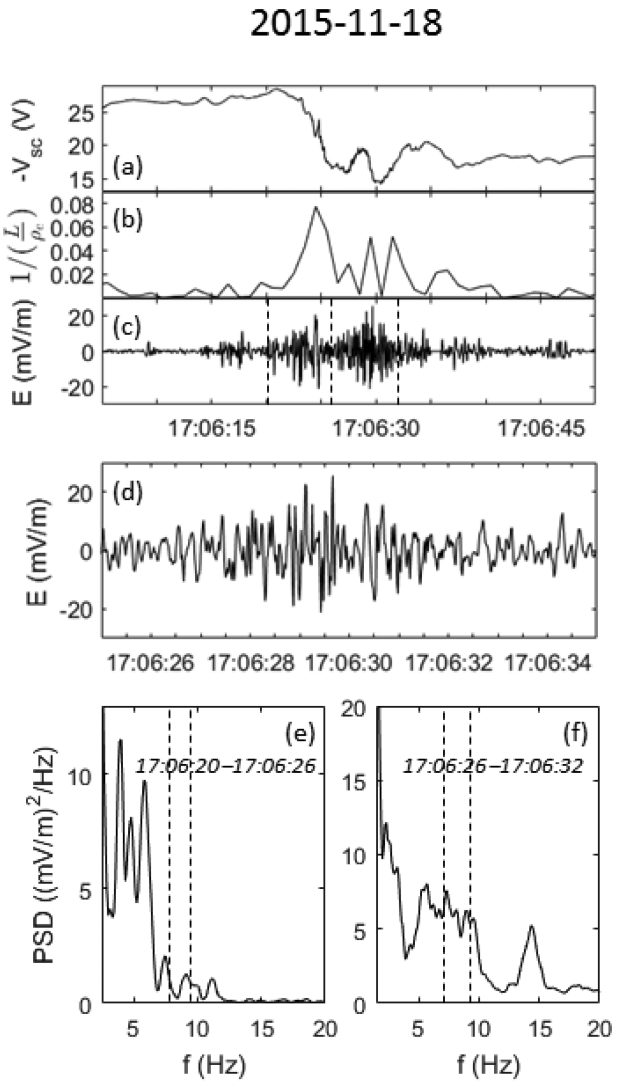

Figure 5. Example of a wave packet at high time resolution from the event in Fig. 4. (a) The negative of the spacecraft potential; (b) the plasma density gradient estimated from the spacecraft potential; (c) the electric field; (d) the electric field at higher time resolution; (e) and (f) wave spectra from selected time periods. The interval of the changing lower hybrid frequency is indicated in the spectra. Waves are typically observed in the interval 0.5 to 1× f_{LH} (see theoretical estimates in Fig. 7). Wave packets in the lower hybrid frequency range are associated with sharp density gradients.

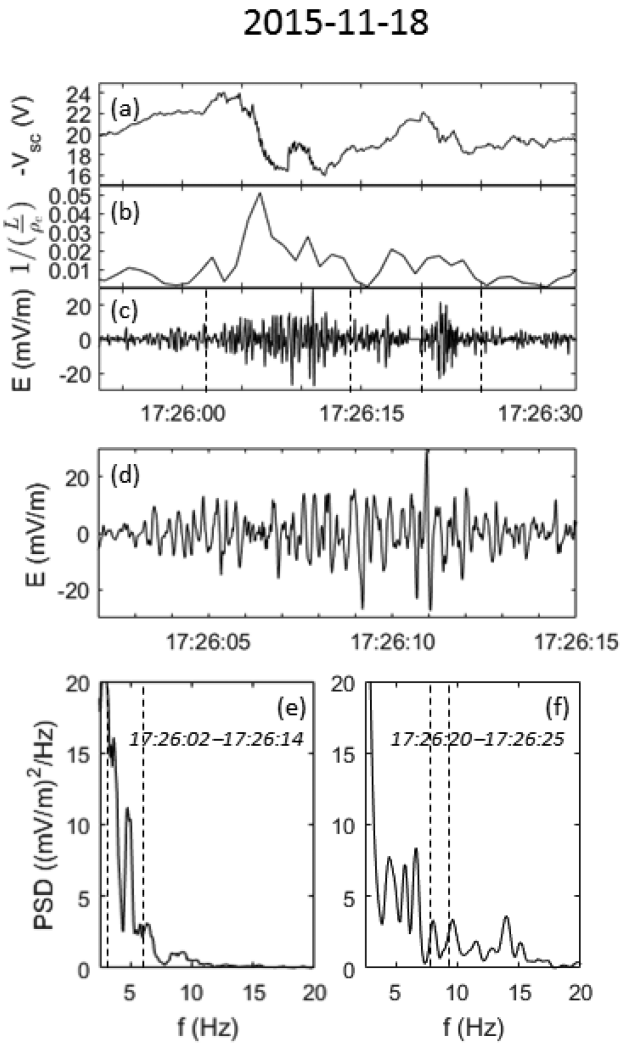

Figure 6. Same panels as in Fig. 5. Again wave packets in the lower hybrid frequency range are associated with sharp density gradients.

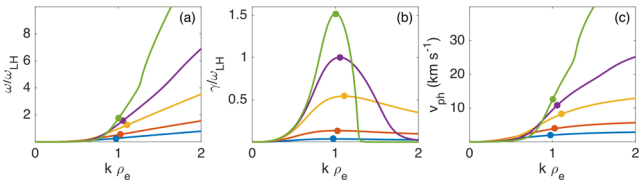

Figure 7. Wave properties and gradients relevant for the observations in Fig. 4. (a) Wave frequency and (b) growth rate (both normalized to the lower hybrid frequency) and (c) phase speed v_{ph}. The circles indicate the points corresponding to peak growth rate. Inverse scalelengths $(L/\rho_e)^{-1}$ of 2.5 × 10^{-3}, 5 × 10^{-3} 1.25 × 10^{-2}, 2.5 × 10^{-2} and 5 × 10^{-2} are indicated by blue, red, gold, purple and green, respectively. Here $f_{LH} \approx 5$ Hz and $\rho_e \approx$ 250 m. The observed large gradients are consistent with significant wave growth.

resolution in Figs 5 and 6. The top three panels of each figure show the average of the LAP probe potentials (an approximation of the negative of the spacecraft potential), the plasma density gradient from the spacecraft potential (equation 12) and the electric field. In addition, electric-field data at even higher resolution and two examples of wave spectra are shown. We find that waves with frequencies in the lower hybrid range are often associated with sharp density gradients.

6.1 Local plasma observations and lower hybrid waves

To calculate growth rates for a range of locally observed gradient scalelengths, Fig. 4, we solve the LHDI dispersion relation, equation (8), numerically. As typical parameters, we use: n_e = 500 cm^{-3} T_i = 10 eV, T_{ew} = 5 eV and B_0 = 30 nT. Since we are interested in the effects of density gradients on wave growth, temperatures and magnetic field are assumed to be constant during the interval, and all electrons are assumed to be warm.

The result is illustrated in Fig. 7. The smallest gradient considered $(L/\rho_e)^{-1} = 2.5 \times 10^{-3}$ is comparable to the average gradient at large distance from the comet in Figs 2 and 3, while the largest gradient $(L/\rho_e)^{-1} = 5 \times 10^{-2}$ is comparable to large gradients close to the comet in Fig. 3. While the smallest gradient produces only marginal

wave growth, the largest gradient produces $\omega \approx \gamma \approx \omega_{LH}$, resulting in significant wave growth within only seconds, and only kilometres of ion drift. Non-linear effects not included in our model are likely to limit the wave growth. We find that locally observed plasma gradients can cause significant wave growth, consistent with local wave observations.

Some waves are not associated with density gradients and may have propagated from nearby regions where gradients are present. Also, our model is not complete and gradients in the magnetic field or local particle jets may also contribute to wave generation. Some density gradients are not associated with waves. Our wave growth estimates assume that the gradient has a significant extent in the azimuthal direction, Fig. 1, at least several wavelengths, i.e. several electron gyroradii (at least some km). The calculated wave growth also depends on the magnetic field and our estimates of ion and electron temperatures and the ion outflow velocity. Thus, we cannot expect a one-to-one correlation between waves and density gradients estimated from local observations. Overall, our wave growth estimates concentrate on the effects of plasma gradients. The observed waves, the observed plasma density gradients and our numerical calculations clearly indicate that gradients are of major importance for the generation of lower hybrid waves around 67P.

7 SUMMARY AND DISCUSSION

In the near plasma environment of 67P and similar comets, waves in the lower hybrid frequency ranges are likely to be common. We consider the situation when the plasma is dominated by magnetized electrons, unmagnetized water group ions and a magnetic field of solar wind origin. This situation is favourable for the generation of waves in the lower hybrid frequency range. Such waves have recently been observed by *Rosetta* (Karlsson et al. 2017; Stenberg Wieser 2017).

We model the near plasma environment of 67P (out to cometocentric distances of a few 100 km) for two levels of neutral outgassing (two heliocentric distances, 1.7 and 2.3 au). In the near plasma environment we consider, ion-neutral collisions are significant and contribute to the demagnetization of the ions. Electron-neutral collisions are important only for higher densities. In our examples, this gives electron cooling (to around 0.1 eV) for the smaller heliocentric distance. This means that mainly cold electrons are present out to cometocentric distances of tens of km, while for larger distances a mixture of cold and warm (5–10 eV) electrons are predicted. When electron-neutral collisions are important, lower hybrid waves are likely to be heavily damped.

Waves in the lower hybrid frequency range can be generated at density gradients, by the LHDI. From our models of average gradients in the near plasma environment, we find that lower hybrid waves are growing, but for larger cometocentric distances not fast enough to be of major importance. The outflowing unmagnetized ions, moving relative to the magnetized electrons can also be unstable to the MTSI, which may produce lower hybrid waves. However, in our example we find that the growth rates are rather low. It is interesting that close to the comet (within tens of km) and for larger heliocentric distances when collisions are not so important, the average gradients are consistent with significant LHDI wave growth.

We investigate *Rosetta* observations from one event (heliocentric distance of 1.7 au, cometocentric distance of 130 km). The observed large-amplitude waves with frequencies in the lower hybrid range are associated with observed local density gradients. These gradients are estimated from variations in the spacecraft potential. We find that many observed local gradients are high enough to cause significant LHDI wave growth. These gradients are likely to be associated with large-scale fluctuations in the plasma structure (much larger than the electron gyroradius and the wavelength). As shown by Eriksson et al. (2017), such large density variations were very common in *Rosetta* data and may relate to the filamentation of the denser plasma closer to the nucleus seen in the hybrid simulations by Koenders et al. (2015).

The comet environment is complex. Effects such as three-dimensional current systems and variations in magnetic field and ion and electron temperatures, not included in our study, can affect the wave growth. Investigations of this can be important for further understanding of the comet plasma environment. Still, our study clearly shows that density gradients can play an important role in the generation of lower hybrid waves around comets.

8 CONCLUSIONS

When the near plasma environment of comet 67P (cometocentric distances out to at least a few hundred km) is dominated by heavy ions from the comet such as H_2O^+, and a magnetic field of solar wind origin, waves in the lower hybrid frequency range are likely to be common. This environment with magnetized electrons and unmagnetized ions is favourable for the generation of lower hybrid waves. These waves are important since they can transfer energy between ions and electrons and reshape the plasma environment. The observed waves we discuss are consistent with generation by the LHDI caused by gradients associated with observed local density fluctuations. These fluctuations are probably associated with filamentation of the denser plasma inside the *Rosetta* orbit. Average large-scale density gradients (LHDI instabilities) and the outflow of ions relative to the magnetized electrons (modified two stream instabilities) can also generate lower hybrid waves, but typically at significantly lower growth rates. Close to the comet, within tens of km, also average gradients can be large enough to cause significant wave growth. Preliminary investigations show that both large local density gradients and lower hybrid waves are common around 67P. A more complete survey of electric-field data from the *Rosetta* LAP instrument is likely to find that LH waves are common, in particular in regions of sharp density gradients.

ACKNOWLEDGEMENTS

We are grateful for support by the Rosetta PI:s and instrument teams. Support by the Swedish National Space Board is acknowledged, including SNSB contracts 109/12, 101/15, 95/15, 96/15, 168/15, 176/15, 166/14 and 175/15. Work on ROSINA/COPS at University of Bern is supported by the State of Bern, the Swiss National Science Foundation and the European Space Agency PRODEX program. Rosetta is a European Space Agency (ESA) mission with contributions from its member states and the National Aeronautics and Space Administration (NASA). This work has made use of the AMDA and RPC Quicklook database, provided by a collaboration between the Centre de Données de la Physique des Plasmas (CDPP) (supported by CNRS, CNES, Observatoire de Paris and Université Paul Sabatier, Toulouse), and Imperial College London (supported by the UK Science and Technology Facilities Council).

REFERENCES

Alfvén H., 1957, Tellus, 9, 92
Altwegg K., Balsiger H., Geiss J., 1999, Space Sci. Rev., 90, 3
Auster H.-U. et al., 2015, Science, 349, aaa5102

Bale S. D., Mozer F. S., Phan T., 2002, Geophys. Res. Lett., 29, 33
Balsiger H. et al., 2007, Space Sci. Rev., 128, 745
Behar et al., 2017, MNRAS, in press
Biermann L., 1951, ZAp, 29, 274
Bingham R., Shapiro V. D., Gil'Man M., Tsytovich V. N., de Angelis U., 1991, Phys. Fluids B, 3, 1728
Bingham R., Shapiro V. D., Quest K. B., Üçer D., Kellett B. J., 2010, in Eliasson B., Shukla P. K., eds, AIP Conf. Proc. Vol. 1306, The Modified Two Stream Instability at Nonmagnetic Planets. Am. Inst. Phys., New York, p. 7
Burch J. L. et al., 2016, Science, 352, aaf2939
Carr C. et al., 2007, Space Sci. Rev., 128, 629
Coroniti F. V. et al., 1986, Geophys. Res. Lett., 13, 869
Cravens T. E., Kozyra J. U., Nagy A. F., Gombosi T. I., Kurtz M., 1987, J. Geophys. Res., 92, 7341
Davidson R. C., Gladd N. T., 1975, Phys. Fluids, 18, 1327
Dyal P., 2006, J. Geophys. Res. Space Phys., 111, A12211
Edberg N. J. T. et al., 2015, Geophys. Res. Lett., 42, 4263
Eriksson A. I. et al., 2007, Space Sci. Rev., 128, 729
Eriksson A. I. et al., 2017, A&A, in press
Fahleson U., 1967, Space Sci. Rev., 7, 238
Fujimoto M., Shinohara I., Kojima H., 2011, Space Sci. Rev., 160, 123
Galand M. et al., 2016, MNRAS, 462, S331
Galeev A. A. et al., 1988, J. Geophys. Res., 93, 7527
Glassmeier K.-H., Boehnhardt H., Koschny D., Kührt E., Richter I., 2007, Space Sci. Rev., 128, 1
Goetz C. et al., 2016, A&A, 588, A24
Goetz C. et al., 2017, MNRAS, in press
Graham D. B. et al., 2017, J. Geophys. Res. Space Phys., 122, 517
Gulkis S. et al., 2015, Science, 347, aaa0709
Gunell H. et al., 2017, A&A, 600, A3
Haser L., 1957, Bull. Soc. R. Sci. Liege, 43, 740
Hässig M. et al., 2015, Science, 347, aaa0276
Hesse M. et al., 2016, Space Sci. Rev., 199, 577
Huba J. D., Gladd N. T., Papadopoulos K., 1977, Geophys. Res. Lett., 4, 125
Itikawa Y., Mason N., 2005, J. Phys. Chem. Ref. Data, 34, 1
Karlsson T. et al., 2017, Geophys. Res. Lett.
Khotyaintsev Y. V., Cully C. M., Vaivads A., André M., Owen C. J., 2011, Phys. Rev. Lett., 106, 165001
Klimov S. I. et al., 1986, Sov. Astron. Lett., 12, 288
Koenders C., Glassmeier K.-H., Richter I., Ranocha H., Motschmann U., 2015, Planet. Space Sci., 105, 101
Koenders C., Perschke C., Goetz C., Richter I., Motschmann U., Glassmeier K. H., 2016, A&A, 594, A66
Krall N. A., Liewer P. C., 1971, Phys. Rev. A, 4, 2094
Lybekk B., Pedersen A., Haaland S., Svenes K., Fazakerley A. N., Masson A., Taylor M. G. G. T., Trotignon J.-G., 2012, J. Geophys. Res. Space Phys., 117, A01217
McBride J. B., Ott E., Boris J. P., Orens J. H., 1972, Phys. Fluids, 15, 2367
Madanian H. et al., 2016, J. Geophys. Res. Space Phys., 121, 5815
Mandt K. E. et al., 2016, MNRAS, 462, S9
Neubauer F. M., 1987, A&A, 187, 73
Neugebauer M., 1990, Rev. Geophys., 28, 231
Nilsson H. et al., 2007, Space Sci. Rev., 128, 671
Nilsson H. et al., 2015a, Science, 347, aaa0571
Nilsson H. et al., 2015b, A&A, 583, A20
Norgren C., Vaivads A., Khotyaintsev Y. V., André M., 2012, Phys. Rev. Lett., 109, 055001
Odelstad E. et al., 2015, Geophys. Res. Lett., 42, 10126
Odelstad E., 2017, MNRAS, in press
Oya H., Morioka A., Miyake W., Smith E. J., Tsurutani B. T., 1986, Nature, 321, 307
Paschmann G., Øieroset M., Phan T., 2013, Space Sci. Rev., 178, 385
Pedersen A. et al., 2008, J. Geophys. Res. Space Phys., 113, A07S33
Priest E., Forbes T., 2000, Magnetic Reconnection. Cambridge Univ. Press, Cambridge
Richardson I. G., Cowley S. W. H., Wenzel K.-P., Scarf F. L., Smith E. J., Tsurutani B. T., Sanderson T. R., Hynds R. J., 1989, Adv. Space Res., 9, 377
Richter I. et al., 2015, Ann. Geophys., 33, 1031
Richter I. et al., 2016, Ann. Geophys., 34, 609
Sauer K., Dubinin E., Baumgärtel K., Tarasov V., 1998, Earth Planets Space, 50, 269
Scarf F., 1989, Plasma Waves and Instabilities at Comets and in Magnetospheres. American Geophysical Union Geophysical Monograph Series, Washington, DC, p. 31
Scarf F. L., Ferdinand V., Coroniti V., Kennel C. F., Gurnett D. A., Ip W.-H., Smith E. J., 1986, Science, 232, 377
Shapiro V. D., Szegö K., Ride S. K., Nagy A. F., Shevchenko V. I., 1995, J. Geophys. Res., 100, 21289
Shapiro V. D., Bingham R., Dawson J. M., Dobe Z., Kellett B. J., Mendis D. A., 1999, J. Geophys. Res., 104, 2537
Stenberg Wieser, 2017, MNRAS, in press
Taylor M. G. G. T., Alexander C., Altobelli N., Fulle M., Fulchignoni M., Grün E., Weissman P., 2015, Science, 347, 387
Trotignon J. G. et al., 2007, Space Sci. Rev., 128, 713
Vaivads A., André M., Buchert S. C., Wahlund J.-E., Fazakerley A. N., Cornilleau-Wehrlin N., 2004, Geophys. Res. Lett., 31, L03804
Vigren E., 2017, MNRAS, in press
Vigren E., Eriksson A. I., 2017, AJ, 153, 150
Vigren E., Galand M., Eriksson A. I., Edberg N. J. T., Odelstad E., Schwartz S. J., 2015, ApJ, 812, 54
Volwerk M. et al., 2016, Ann. Geophys., 34, 1
Winske D., 1988, J. Geophys. Res., 93, 2539
Winske D., 1989, Phys. Fluids B, 1, 1900
Wu C. S., Winske D., Papadopoulos K., Zhou Y. M., Tsai S. T., Guo S. C., 1983, Phys. Fluids, 26, 1259
Yang L., Paulsson J. J. P., Simon Wedlund C., Odelstad E., Edberg N. J. T., Koenders C., Eriksson A. I., Miloch W. J., 2016, MNRAS, 462, S33
Zhou M. et al., 2009, J. Geophys. Res. Space Phys., 114, A02216

This paper has been typeset from a TEX/LATEX file prepared by the author.